Enhancing Multifunctionality: Optimal Properties of Iron-Oxide-Reinforced Polyvinylidene Difluoride Unveiled Through Full Atom Molecular Dynamics Simulations

Fahmi Bedoui, Mehdi Sahihi, Andres Jaramillo-Botero, William Goddard

Enhancing Multifunctionality: Optimal Properties of Iron-Oxide Reinforced Polyvinylidene Difluoride Unveiled Through Full Atom Molecular Dynamics Simulations

Fahmi BEDOUI[1,2], Mehdi Sahihi[3], Andres Jaramillo-Botero[2], William A. Goddard III[2]

[1] Alliance Sorbonne Université, Université de Technologie de Compiègne, Laboratoire Roberval, Compiègne, France

[2] Materials and Process Simulation Center, California Institute of Technology, Pasadena, CA, USA

[3] Université Clermont Auvergne, CNRS, Clermont Auvergne INP, Institut de Chimie de Clermont-Ferrand, F-63000 Clermont-Ferrand, France

Abstract

Nanocomposites made of magnetite (Fe_3O_4) nanoparticles (NP)s with different surface chemistry and Polyvinyl difluoride (PVDF) polymer were investigated using full atom molecular dynamics (MD) simulation. NPs with hydroxyl (OH), hexanoic, and oleic acid terminations were considered in this study. The effect of each surface chemistry was investigated in terms of the mechanical properties, the distribution of the internal energy around the NP, and the chain polarization gradient from the interface to the bulk. From this investigation, we find that oleic acid termination although the most popular, is-less favorable for interfacial interaction and local polarization. The OH-terminated NP results in the best configuration for the properties investigated. The hexanoic acid-grafted NP presents a good compromise. Hydrogen bonding governs the induced response of the nanocomposites. Although the hexanoic acid grafted NP presents less hydrogen bonding than the OH-terminated case, the conformation of the hexanoic acid acts as a mobility flow inhibitor, leading to performance comparable to the OH-terminated NP composite. This work led to investigating routes to make nanocomposite materials with optimized properties. These results shed light on

the multiple combinations offered by nanocomposites that go beyond the conventional effects of size.

Introduction

Nano-reinforced polymers have received considerable attention, from both industrial and academic points of view. In addition to the shape and mechanical properties offered by nanoparticles, their nano size also contributes to enhancement of the composite mechanical properties. The high surface-to-volume offered by NP contributes to higher interactions with the surrounding matrix. This increased surface-to-volume ratio induced by small particles favored induction of a more ordered structure at the interface, leading to a stiffer interface that contributes to enhancing the global mechanical properties*[1–7]*. Interaction at the interface affects such other properties such as piezoelectricity [8–10]. In this specific configuration, interfacial interactions for PVDF-reinforced polymers affects chain polarization at the interface, leading to either increased or decreased induced piezoelectric properties of the composite[11]. Thus, size effects that were meant for modifying mechanical properties appear not to be universally beneficial for other properties. Note that NPs come always with chemical surfactants grafted at their surfaces[12–16]. The use of surfactants is meant to control the NP growth and therefore their form and size[17]. It is through the grafted surfactant at the interface that the NP-polymer interacts with the environment [18]. The nature of these interactions needs to be fully understood in order to optimize the response of the composite. Controlling such interactions could allow optimization of more than a single property (mechanical for instance) to reach multiple optimum properties including electric, thermal, and other properties. Such interactions occur at a nano-length scale making it impossible to extract such interactions from experiments. Many different NP-polymer interaction configurations exist. Given the large number of possibilities, it is hard to cover all possible combinations in a reasonable time. There

is therefore a need to simulate the NP-Surfactant-Polymer interaction beforehand to help guide the experiments in the most promising directions. Among various modeling approaches, atomistic is the most relevant for this case, since it can capture short time and length scales. Some publications already discuss the effect of surfactants (attached on the NP surface) on polymeric nanocomposites[19–22], however, most publications target the understanding of local conformation or induced physical properties but not (as far as authors know) how to optimize combined properties at the macroscale, such as mechanical and piezoelectric properties.

This paper addresses this point, with a particular focus on the case of PVDF with Fe_3O_4 NPs. The effect of NP surface chemistry on both mechanical and piezoelectric properties are investigated to understand the underlying mechanisms of the interfacial interaction between the NP and the surrounding polymeric matrix. We previously optimized a fixed charge forcefield [11]for each component that we will now use to examine local conformation, interfacial interaction, and mechanical response. Among the different configurations explored, we will classify them from the best to the worst to help chemist in their NP synthesis choices.

2. Computational procedure

The following procedure was used to build and simulate the interaction of α-PVDF with functionalized Fe_3O_4 NPs:

2.1. Construction and functionalization of the magnetite NPs

The unit cell of Fe_3O_4 crystal (CIF number 1011032) was downloaded from the open crystallography database (http://www.crystallography.net/)[23] and was transformed to a magnetite NP with a diameter of 2.5 nm using the web-based crystallographic tool NanoCrystal, (http://nanocrystal.vi-seem.eu/)[24]. After preparation of the magnetite NP, its surface was modified using the following procedure:

1) Removal of Fe^{2+} and Fe^{3+} Iron atoms with less than 4 and 6 bonds, respectively, to eliminate the crystal defects of the magnetite;

2) Replaced all oxygen atoms with only one bond at the magnetite surface by OH groups;
3) Replaced 20% of OH groups by hexanoic and oleic acid groups to prepare three different types of magnetite NPs with different surface chemistries (one sample with 100% of OH-termination and two other samples with 20% of various carboxylic acid modifications which is equal to about 1.43 chain.nm^{-2}).

Before modification of the magnetite surface, the chemical structures of water, hexanoic acid, and oleic acid were optimized as in our previous work[11 10]. Figure 1 represents the final structure of hexanoic acid and oleic acid functionalized magnetite NPs.

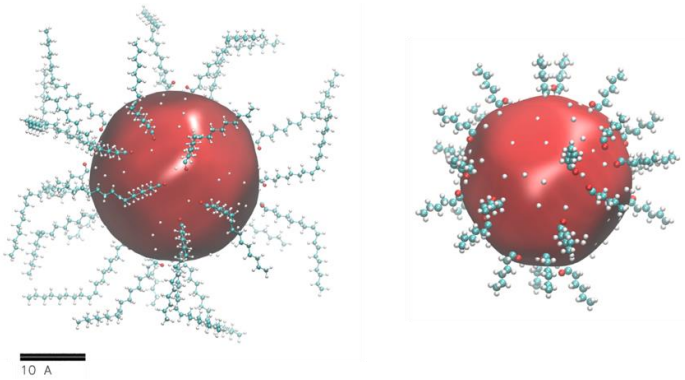

Figure 1. Magnetite NPs with different surface chemistry: (left) 20% oleic termination and (right) 20% hexanoic acid termination.

2.2. Construction of Fe_3O_4-PVDF systems

The known crystal structure of α-PVDF was used[25] to prepare the structure of the PVDF chain using Avogadro[26]. A single chain of PVDF contains 100 monomers and 34 copies of single chain PVDF were placed around the NPs randomly to achieve the volume fraction of 4%.

2.3. MD simulation of Fe_3O_4-PVDF systems

All MD simulations were carried out using the GROMACS version 5.0.7 simulation package [27,28]. The force field parameters from our previous work were used for magnetite and PVDF[11]. The systems were placed in the center of the cubic box with the minimum distance between the system and the box surface set to 1.0 nm. The core part of the NPs (NPs excluding their surface treatments) was geometrically frozen during the simulations to approximate a realistic hard core

of NPs. Integration of the equations of motion was done using a time step of 0.5 fs with full periodic boundary conditions (PBC) applied along the three Cartesian directions. The systems were energy minimized using the steepest descent method, with 10^{-6} kJ /mol and kJ /mol nm for energy difference and RMS force, respectively) convergence criteria, and were equilibrated for 1 ns using an NVT ensemble at 300 K with a Berendsen thermostat[29] with a damping constant of 0.1 ps. After the NVT equilibration step, to be certain that PVDF chains can overcome the potential barrier and rotate freely, the PVDF chains were heated from 300 K to 600 K over 6 ns and then were cooled down to 300 K at the same rate as the heating step. Finally, we performed 10 ns of NVT MD simulation at 300 K. During the simulation a we applied a 1.0 nm cutoff for van der Waals (vdW) and Coulomb interactions and used the particle mesh Ewald (PME) method[30,31] for long-range electrostatics. The LINCS method[32] was used as a constraint algorithm. Three independent replica simulations were conducted for each system to ensure robustness and reliability of the results. In each replica, the system was simulated starting from different initial velocities. Following the completion of the simulations, dipole moments were calculated for each replica, and these values were averaged across the independent simulations. Averaging dipole moments helps mitigate statistical fluctuations and provides a more accurate representation of the system's average dipole moment, which is essential for understanding its electrostatic properties and behavior.

3. Results and discussion

3.1.Chains conformation

As chain cohesiveness from the interface to the bulk seemed to be dependent on the NP surface, we investigated their conformations.

We investigated the average dipole moment (μ) of the α-PVDF chains, to understand the driving mechanism of the α- to β-phase transition during the interaction with Fe_3O_4 NPs. This employed the "gmd dipoles" module of GROMACS for dipole moment calculations. This module

calculates the dipole moment of a molecular system based on the positions and charges of atoms. It reads the atomic coordinates and charges from the trajectory and determines the center of charge of the system. This center of charge is essentially the weighted average of the atomic positions, where the weights are given by the atomic charges. Once the center of charge is computed, the module calculates the dipole moment vector.

After the equilibration process, we carried NVT simulations for 10 ns, averaging and calculating the dipole moments of PVDF chains at various distances from the interface (figure 2). From these calculations, it appears that NP surface chemistry governs the PVDF chain conformation. Greater access to oxygen and OH termination-rich surfaces favor the TT conformation as evidenced by the local dipole moment. Indeed, the OH termination system presents the highest polarization at the interface followed by the hexanoic acid and then the oleic acid. OH termination is favorable for the PVDF chains to interact with the oxygen-rich iron oxide surface. For both oxygen and fluorine, the repulsion between the two atoms favors triggering dihedral rotation to induce a full trans configuration at the interface. Similarly, access to OH termination favors hydrogen bonding, which could trigger the formation of the full trans configuration.

Those favorable interaction conditions vanish with oleic acid-grafted NP. Oleic acid has long chains and the double bond leads to bent molecules which, despite the only 20% grafting density will act to shade the structure preventing oxygen-fluorine repulsion from one side and OH – fluorine on the other. Together these conditions inhibit the formation of the full trans configurations leading to the lowest interfacial polarization.

Hexanoic acid is much shorter than oleic one and has a straighter chain. With a grafting density of 20%, the linear hexanoic acid structure provides space for the PVDF chain to interact with the iron oxide surface. Indeed this has been observed on an iron oxide slab grafted with hexanoic acid and interacting with the PVDF polymeric chain layer[10,11].

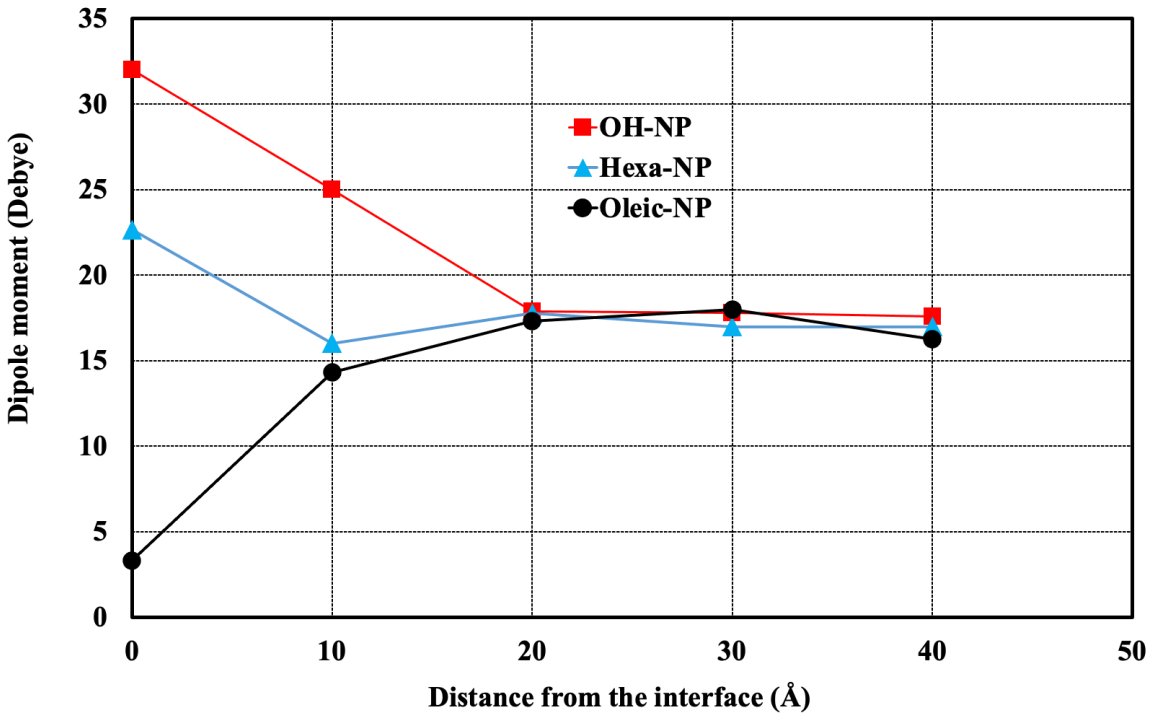

Figure 2: molecular dipole moment from the interface to the bulk for the various grafted NP-based composites.

147

148 ***3.2. Thermodynamic properties***

149 To analyze the thermodynamic properties of our systems, we applied the two-phase
150 thermodynamic analysis (2PT)[33,34] along the trajectories. The 2PT density of states is obtained
151 from the Fourier transform of the velocity autocorrelation function[35,36], which can used to
152 derive local entropy and free energy at the atomic scale, or for an ensemble of atoms, or for
153 molecular chains. From the MD trajectory, we obtain the spectral density of the system, [35] as
154 follows:

155 $$s_j^k(\nu) = \lim_{\tau\to\infty} \left| \int_{-\tau}^{+\tau} V_j^k(t)\, e^{-i2\pi\nu t} dt \right|^2 \quad (1)$$

156 $$S(\nu) = \frac{2}{K\,T} \sum_{j=1}^{N} \sum_{k=1}^{3} m_j s_j^k\,(\nu) \quad (2)$$

Where $V_j^k(t)$ is the *k*-component of velocity vector of atom *j* at time *t, mj* is the mass of atom *j*, and *N* is total number of atoms of the system. The physical significance of *S*(υ) is that it represents the density of normal modes of the system at frequency υ.

From the density of states we obtain the canonical partition function *Q:*

$$ln(Q) = \int_0^\infty dvS(v)Ln(q);\ \ q = \frac{\exp(-\frac{\beta hv}{2})}{1-\exp(-\frac{\beta hv}{2})}\ ;\ \beta = 1/kT \quad (3)$$

where *h* represents the Plank constant, k the Boltzmann constant, and T temperature in kelvin. Integrating the density of states function according to Lin et al [36] leads to a quantitative estimate of the thermodynamic properties (internal energy, entropy, Helmholtz free energy, etc.) of the system, as follows:

$$E = E_0 + T\beta^{-1}\left(\frac{\partial Ln(Q)}{\partial T}\right)_{N,V} = E_0 + \beta^{-1}\int_0^\infty S(v)W_E(v)dv \quad (4)$$

$$S = KLn(Q) + \beta^{-1}\left(\frac{\partial Ln(Q)}{\partial T}\right)_{N,V} = K\int_0^\infty S(v)W_S(v)dv \quad (5)$$

$$A = E_0 - \beta^{-1}Ln(Q) = V_0 + \beta^{-1}\int_0^\infty S(v)W_A dv \quad (6)$$

where E_0 is the potential energy at 0 K, and W_E, W_S and W_A are the internal energy, entropy, and Helmholtz free energy weighting functions, as in (7)-(9):

$$W_E(v) = \frac{\beta hv}{2} + \frac{\beta hv}{\exp(\beta hv)-1} \quad (7)$$

$$W_S(v) = \frac{\beta hv}{\exp(\beta hv)-1} - ln[1-\exp(-\beta hv)] \quad (8)$$

$$W_A(v) = ln[\frac{1-\exp(\beta hv)}{\exp(-\beta hv)}] \quad (9)$$

This 2PT approach gives access to atom-based energy decompositions, based on atomic velocities, which can be extended to groups of atoms. In our case, atom groups were defined as for the chain conformation study, namely concentric domains starting from the NP-Polymer interface toward the bulk. After the 10 ns NPT equilibration, several 20 ps trajectories were analyzed using 2PT, for all the predefined atom groups; from the interface to the bulk (figure 3).

Using this analysis, we investigated the three composite samples. The internal energy was derived for all the concentric layers starting from the interface toward the bulk. The OH-terminated NP appears to lead to internally cohesive layers with the highest internal energy. The Oleic terminated NP system leads to the opposite trend. The interfacial layer seems to be the less cohesive with the polymeric layer interacting less with the NP. The long oleic chains have no specific affinity with PVDF chains so that they acting as disturbers to the chain interaction.

The hexanoic terminated case leads to intermediate character. These short ligands provide the possibility of PVDF chains interacting directly with the magnetite surface. The magnetite surface is covered with hexanoic acid at a density of 20%. The remaining open spots were terminated with OH. Being much shorter than oleic acid, the hexanoic acid ligand leaves more space for the PVDF chain to interact with the oxygen and OH-rich NP surface, leading to more cohesively packed chains, which in turn provide more stable and cohesive layers.

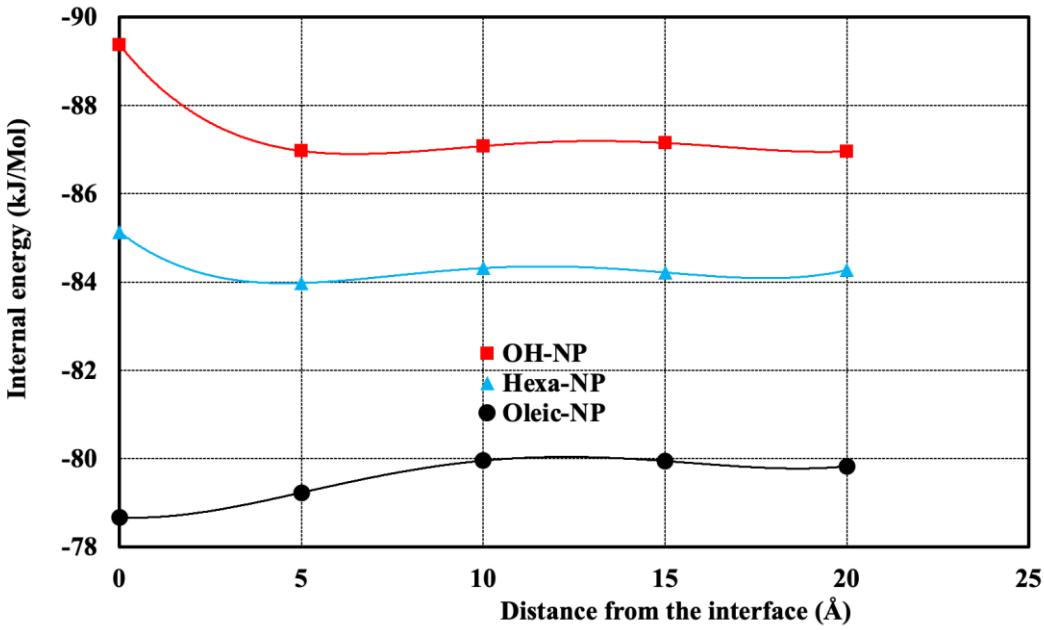

Figure 3: Internal energy distribution from the interface to the bulk for the different grafted NP based composites.

193

194 ***3.3. Mechanical properties***

195 The polymeric matrix and the three composites were sheared at identical constant shearing
196 rates. Predefined LAMMPS function (fix deform) was used to perform shearing tests. It
197 Changes the shape of the simulation box during a dynamics run. In our case, while imposing
198 deformation on xy, yz or xz, constant pressure was imposed on the non-deformed facets of the
199 simulation box. The deformation was run under the NPT ensemble. For each deformed system,
200 the shear modulus was determined as the ratio of the stress shear component on the
201 correspondent deformation as follows (in the case of xy deformation) $G = \tau_{xy}/\gamma_{xy}$. The stress-
202 strain response of the four samples is presented in Figure 4. This result is an average of three
203 tests along xy, xz, and yz shearing (figure 3). The dashed lines provide polynomial
204 interpolations to help follow the data. We see that adding nanoparticles enhances drastically the
205 strength of the polymeric material regardless of which ligand is grafted onto the surface.
206 However, the longer the chain the less the stiffening effect. This is consistent with internal
207 energy distribution at the interface. Indeed, less cohesive interfaces tend to deform at low
208 energy leading to a softer material.

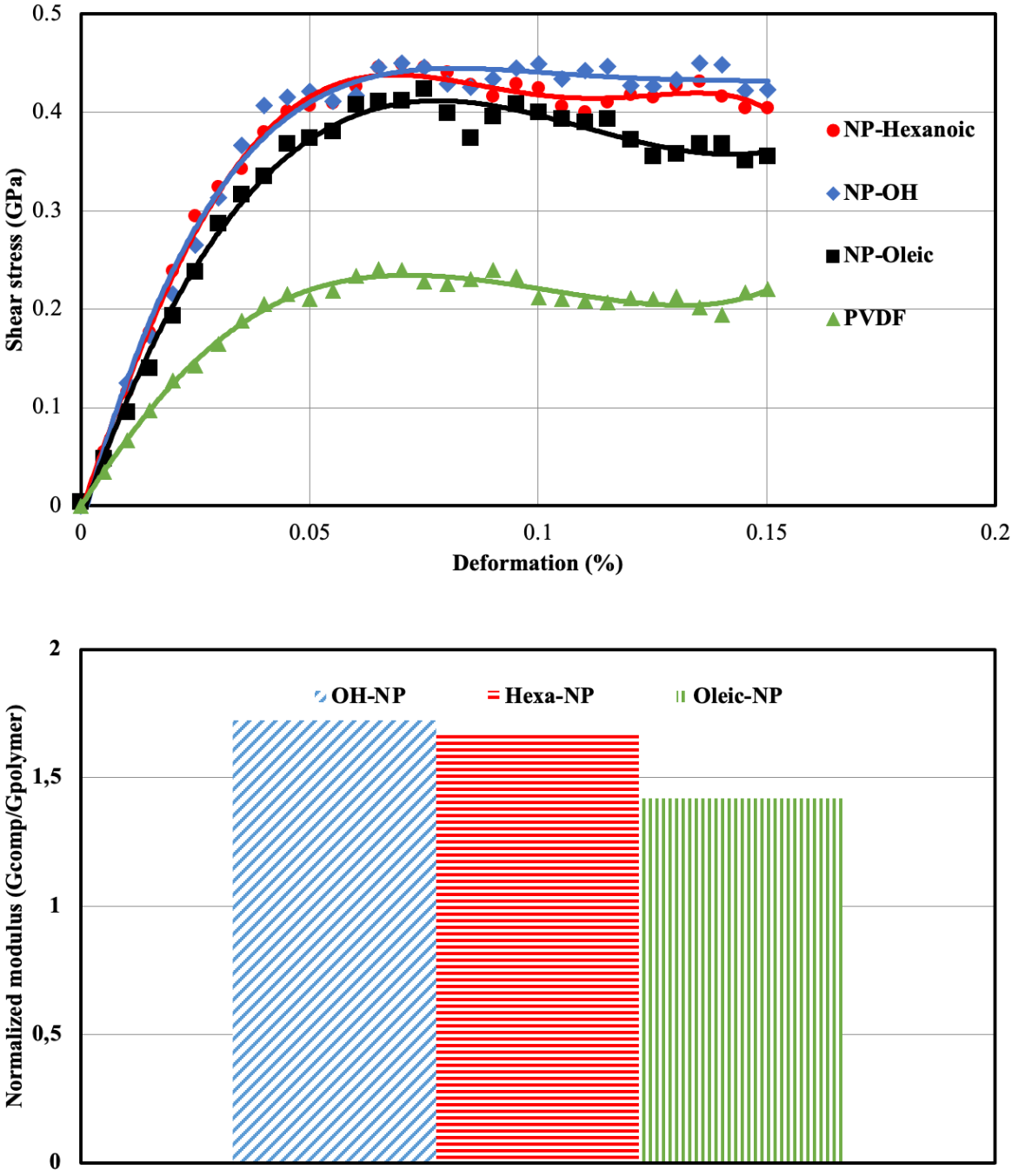

Figure 4: **Top** Mechanical response (shear stress versus strain) of the different grafted NP-based composites (lines provide fitting curves to help follow the data); **Bottom** normalized shear modulus (Composite modulus/polymer modulus)

The OH-terminated NP provides the largest stiffening with a 72% increase in the composite shear modulus. The hexanoic acid terminated NP induces a 67% increase while the Oleic acid terminated NP is much lower with a 42% increase. The three composites have a constant NP volume fraction. This result is consistent with the internal energy profile. Indeed, the OH-terminated NP favors hydrogen bonding interaction in addition to the van der Waals interactions.

A NP surface rich in hydrogen favors hydrogen bonding with the PVDF chains. Thus, the OH-terminated NPs provides the largest hydrogen bonding. These hydrogen bonds seem to be maintained throughout the stretching as illustrated in figure 5. The hydrogen bonds were identified in the post-treatment step using VMD software. Hydrogen bonds were defined between atom donor (Oxygen on the NP surface bonded to hydrogen) and receptor (fluorine atom in the polymer chain). The OF distance must be less than 3.5 Å and the donor-H-acceptor angle must be greater than 120 degrees. With 20% hexanoic acid grafting the hydrogen bonding decreases substantially. Indeed, the presence of grafted molecules prevents PVDF chains from getting close enough to the surface, therefore decreasing the possibility for hydrogen bonds. Similarly, the longer chains of oleic acid substantially prevent interactions between the PVDF chains and the NP surface, with very few hydrogen bonds.

3.4.Discussion

Based on the hydrogen bonding results, we could expect that the mechanical properties of the OH-terminated NP composites would be substantially higher than the hexanoic-terminated NP composite but we find that this is not necessarily the case (figure 5). To explore the possible origin of this unexpected result, we investigated the NP angular velocity during the stretching for all the composite samples. While shearing the system, the polymeric chains are subject to material flow. This material flow can induce rotation of the NP. These results suggest that the oleic acid grafted NP induces more rotation. Indeed, our simulations and previous studies[10,11],

show that the double bond in the oleic acid chain tends to bend the acid chain, thereby covering the NP. In this configuration, the difference in inertia of the NP and the surrounding chain leads the NP to gain momentum and rotate. Since the NP interacts less with the surrounding matrix, the rotation is facilitated.

For the OH-terminated NP, the strong interaction with the matrix through the hydrogen bonds limit this rotation (figure 5). This induces more restrictions in the mobility surrounding the NP resulting in a higher mechanical response.

For the Hexanoic grafted NP, the angular velocity profile is close to the OH terminated NP case even though there is less hydrogen bonding at the interface (figure 5). The explanation for this behavior lies in the conformation of the grafted chain on the NP surface. Indeed, in previous work, we showed that hexanoic acid remains straight on the surface, unlike oleic acid which bends toward covering the NP surface. This forms an obstacle for polymeric chains to flow in the hexanoic case. With less flow on the interface, rotation is inhibited.

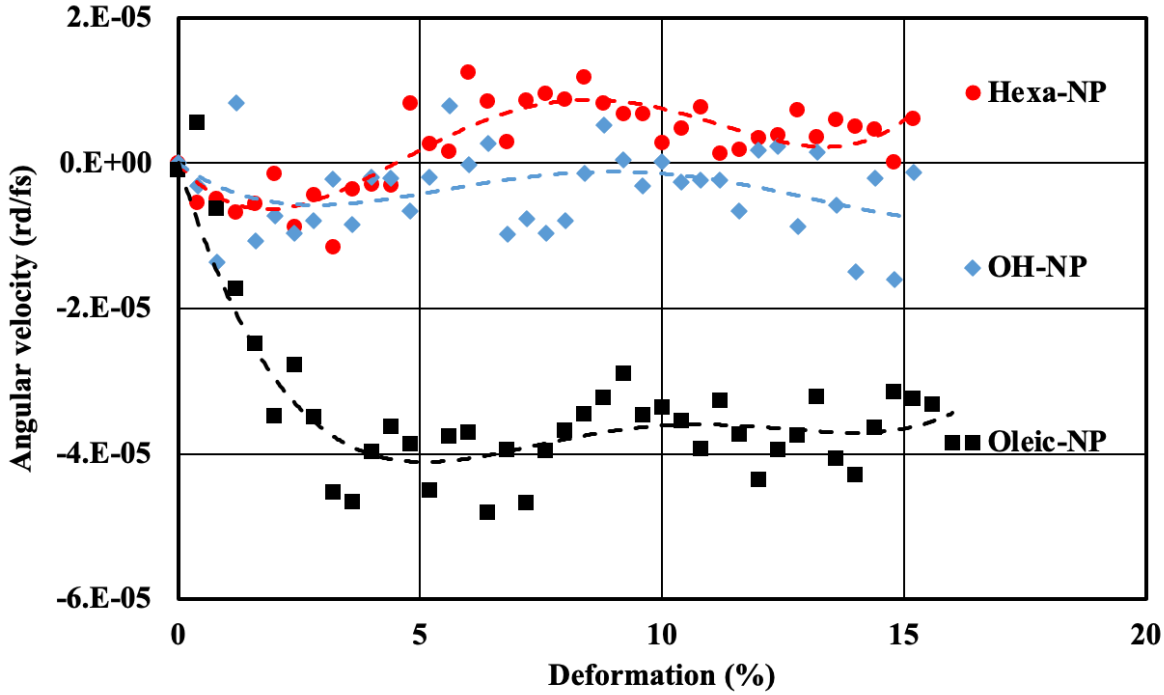

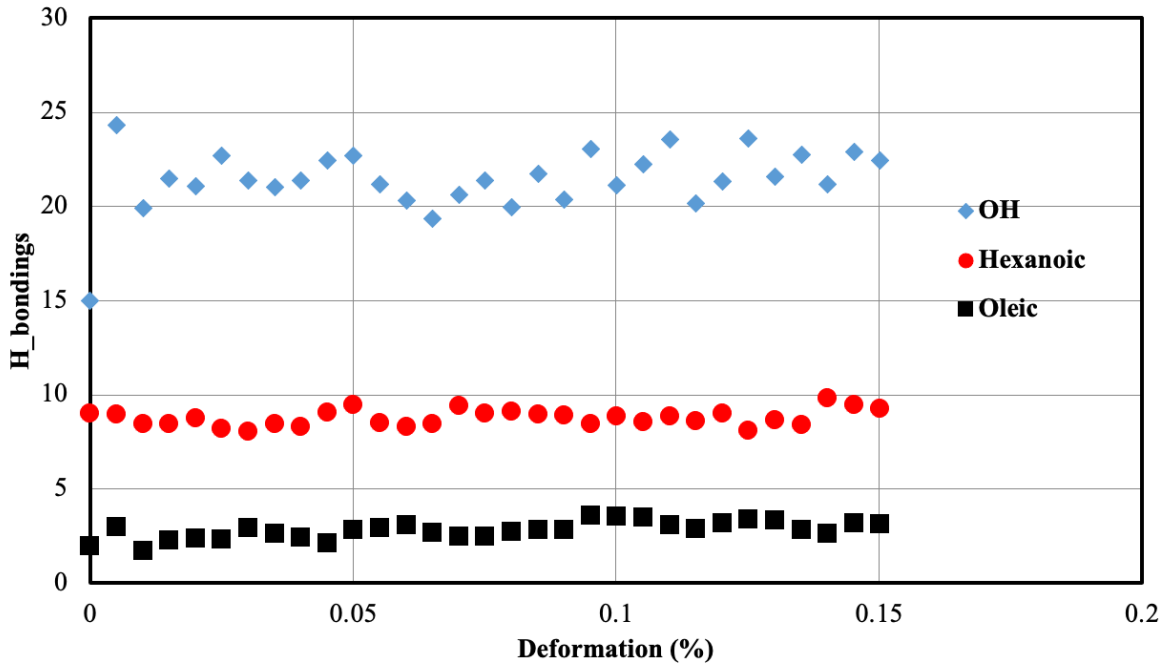

Figure 5: **Top** NP angular velocity (the dashed lines are trend curves to help read the data) and **Bottom** hydrogen bonding sites under shearing for the different grafted NP-based composites;

Shearing induces chains to slip around the NP. Higher interfacial interaction prohibits this slipping, leading to higher induced stress as the system is deformed.

The physical picture we can draw from these results is that for nano-reinforced polymers, factors other than size, matter. Indeed, the nanosize particles exhibit a high interfacial surface through which the matrix-NP interaction occurs (figure 6). At the interfacial level, the surface chemistry of the NP plays a paramount role. Indeed, it governs the way the surrounding polymeric chains will be packed thereby affecting mobility[37]. Such mobility restrictions will influence their contributions to the global mechanical response [18]. In our case, the OH-terminated NP offers a highly favorable (oxygen and OH termination-rich) surface configuration for the PVDF chain to interact with the NP leading to a more probable full trans configuration[38]. During the deformation, the NP inertia along with the hydrogen bonding interaction prevents the NP from rotating making it follow the sheared flow. As a result, the OH-terminated NP-based composite presents a stiffer response along with high polarization at the interface. The hexanoic acid terminated NP, presents a straight grafted chain providing sufficient room for the PVDF chains to interact with the available OH termination and with the oxygen-rich NP surface. These interactions are much less than those available in the OH-terminated NP. Nonetheless, the hexanoic case presents mechanical stiffness and NP rotation close to the OH termination case. We believe that the straight grafted chain acts as rotation blockers in a card-like system.

For the Oleic acid grafted NP-based composite, due to the double bond present in the oleic acid chain, the ligand is naturally bent toward the surface therefore covering the surface and preventing the polymeric chain from fully interacting with the NP. This results in less hydrogen bonding, leading to less cohesive energy at the interface. This makes the NP free to follow the shearing flow as observed through the NP angular rotation. As a result, there is less stiffness compared to the two other cases.

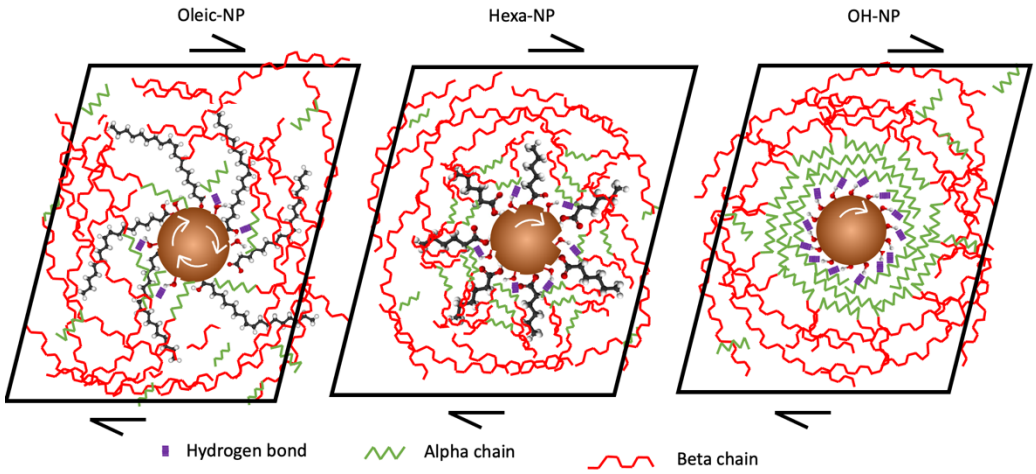

Figure 6: Schematic representation of NP-matrix interaction, the induced chain conformation and NP rotation during the shearing deformation. (From left to right: 20% oleic acid, 20% hexanoic acid and pure OH terminated NPs.)

Conclusion

In summary, we explored the effect of NP surface chemistry on both mechanical macroscopic composite responses and chain polarization of the surrounding matrix. The commonly used oleic acid grafted ligand induces lower interfacial interaction, leading to low internal energy at the interface and therefore lower mechanical properties, when compared to the other terminations. The best configuration, from our simulation, is the OH-terminated NP. Although this case may be difficult to synthesize because such a NP may not be compatible with a solvent-based process. Hexanoic acid grafted ligand presents a good compromise since it favors moderate interaction due to its straight conformation. In addition, this configuration acts as a shear flow inhibitor leading to better mechanical properties than the oleic case. These results shed light on mechanisms that are difficult to extract experimentally, opening new possibilities for improved polymer nanocomposite development through atomistic guided synthesis.

Acknowledgment

The authors acknowledge the financial support from the Alliance Sorbonne University, Université de Technologie de Compiègne, and the Materials and Process Simulation Center at CalTech through the LEEGO project. F. Bedoui acknowledges the financial support from the Alliance Sorbonne University through the INTIMATE Emergence-funded project. The authors greatfully thanlk Dr. Tod Pascal from the University of California San Diego for his help on the 2-PT computation.

References

(1) Papon, A.; Saalwächter, K.; Schäler, K.; Guy, L.; Lequeux, F.; Montes, H. Low-Field NMR Investigations of Nanocomposites: Polymer Dynamics and Network Effects. *Macromolecules* **2011**, *44* (4), 913–922. https://doi.org/10.1021/ma102486x.

(2) A. S.Blivi; F. Benhui; J. Bai; D. Kondo; F. Bedoui. Experimental Evidence of Size Effect in Nano-Reinforced Polymers: Case of Silica Reinforced PMMA. *Polym. Test.* **2016**, *56*, 337–343.

(3) Brown, D.; Marcadon, V.; Mélé, P.; Albérola, N. D. Effect of Filler Particle Size on the Properties of Model Nanocomposites. *Macromolecules* **2008**, *41* (4), 1499–1511. https://doi.org/10.1021/ma701940j.

(4) Blivi, A. S.; Bedoui, F.; Weigand, S.; Kondo, D. Multiscale Analysis of Nanoparticles Size Effects on Thermal, Elastic, and Viscoelastic Properties of Nano-Reinforced Polymers. *Polym. Eng. Sci.* **2020**, *60* (8), 1773–1784. https://doi.org/10.1002/pen.25413.

(5) Berriot, J.; Montes, H.; Lequeux, F.; Long, D.; Sotta, P. Evidence for the Shift of the Glass Transition near the Particles in Silica-Filled Elastomers. *Macromolecules* **2002**, *35* (26), 9756–9762. https://doi.org/10.1021/ma0212700.

(6) Fu, J.; Shi, L.; Zhang, D.; Zhong, Q.; Chen, Y. Effect of Nanoparticles on the Performance of Thermally Conductive Epoxy Adhesives. *Polym. Eng. Sci.* **2010**, *50* (9), 1809–1819. https://doi.org/10.1002/pen.21705.

(7) Li, Y. Effect of Nano Inclusions on the Structural and Physical Properties of Polyethylene Polymer Matrix. *Polymer* **2011**, *52* (10), 2310–2318. https://doi.org/10.1016/j.polymer.2011.03.025.

(8) Calavalle, F.; Zaccaria, M.; Selleri, G.; Cramer, T.; Fabiani, D.; Fraboni, B. Piezoelectric and Electrostatic Properties of Electrospun PVDF-TrFE Nanofibers and Their Role in Electromechanical Transduction in Nanogenerators and Strain Sensors. *Macromol. Mater. Eng.* **2020**, *305* (7), 2000162. https://doi.org/10.1002/mame.202000162.

(9) Barrau, S.; Ferri, A.; Da Costa, A.; Defebvin, J.; Leroy, S.; Desfeux, R.; Lefebvre, J.-M. Nanoscale Investigations of α- and γ-Crystal Phases in PVDF-Based Nanocomposites. *ACS Appl. Mater. Interfaces* **2018**, *10* (15), 13092–13099. https://doi.org/10.1021/acsami.8b02172.

(10) Navarro Oliva, F. S.; Sahihi, M.; Lenglet, L.; Ospina, A.; Guenin, E.; Jaramillo-Botero, A.; Goddard, W. A.; Bedoui, F. Nanoparticle Size and Surface Chemistry Effects on Mechanical and Physical Properties of Nano-Reinforced Polymers: The Case of PVDF-

Fe3O4 Nano-Composites. *Polym. Test.* **2023**, *117*, 107851. https://doi.org/10.1016/j.polymertesting.2022.107851.
(11) Sahihi, M.; Jaramillo-Botero, A.; Goddard, W. A. I.; Bedoui, F. Interfacial Interactions in a Model Composite Material: Insights into α → β Phase Transition of the Magnetite Reinforced Poly(Vinylidene Fluoride) Systems by All-Atom Molecular Dynamics Simulation. *J. Phys. Chem. C* **2021**, *125* (39), 21635–21644. https://doi.org/10.1021/acs.jpcc.1c05894.
(12) Lisiecki, I.; Pileni, M. P. Synthesis of Well-Defined and Low Size Distribution Cobalt Nanocrystals: The Limited Influence of Reverse Micelles. *Langmuir* **2003**, *19* (22), 9486–9489. https://doi.org/10.1021/la0301386.
(13) A-T Ngo; Costanzo S; Albouy P-A; Salzemann C; Richardi J; Lisiecki I. Formation of Colloidal Crystals of Dodecanoic Acid Coated γ-Fe2O3: Experimental and Theoretical Investigations. *Colloids Surf.* **2019**, *A* (560), 270–277.
(14) Baaziz, W.; Pichon, B. P.; Fleutot, S.; Liu, Y.; Lefevre, C.; Greneche, J.-M.; Toumi, M.; Mhiri, T.; Begin-Colin, S. Magnetic Iron Oxide Nanoparticles: Reproducible Tuning of the Size and Nanosized-Dependent Composition, Defects, and Spin Canting. *J. Phys. Chem. C* **2014**, *118* (7), 3795–3810. https://doi.org/10.1021/jp411481p.
(15) Albahrani, S. M. B.; Simon, G.; Ayrinhac, S.; Gauthier, M.; Decremps, F.; Lisiecki, I.; Constanzo, S.; Colomban, P. Stability of Lauric Acid at High Pressure Studied by Raman Spectroscopy and Picosecond Acoustics. *Eur. Phys. J. B* **2019**, *92* (2), 35. https://doi.org/10.1140/epjb/e2018-90479-7.
(16) Hyeon, T.; Lee, S. S.; Park, J.; Chung, Y.; Na, H. B. Synthesis of Highly Crystalline and Monodisperse Maghemite Nanocrystallites without a Size-Selection Process. *J. Am. Chem. Soc.* **2001**, *123* (51), 12798–12801. https://doi.org/10.1021/ja016812s.
(17) Meftah, S.; Ngo, A.-T.; Shahmanesh, A.; Courty, A.; Kondo, D.; Bedoui, F.; Lisiecki, I. Striking Effect of the Iron Stearate Purity on the Shape and Size of Maghemite Nanoparticles. *Colloids Surf. Physicochem. Eng. Asp.* **2024**, *680*, 132689. https://doi.org/10.1016/j.colsurfa.2023.132689.
(18) F. Bedoui; A. Jaramillo-Botero; Tod A. Pascal; William A. Goddard-III. Focus on the Deformation Mechanism at the Interfacial Layer in Nano-Reinforced Polymers: A Molecular Dynamics Study of Silica - Poly(Methyl Methacrylate) Nano-Composite. *Mech. Mater.* **2021**, *159*, 103903. https://doi.org/10.1016/j.mechmat.2021.103903.
(19) Grubbs, R. B. Roles of Polymer Ligands in Nanoparticle Stabilization. *Polym. Rev.* **2007**, *47* (2), 197–215. https://doi.org/10.1080/15583720701271245.
(20) Al-Shatty, W.; Campana, M.; Alexander, S.; Barron, A. R. Interaction of Surface-Modified Alumina Nanoparticles and Surfactants at an Oil/Water Interface: A Neutron Reflectometry, Scattering, and Enhanced Oil Recovery Study. *ACS Appl. Mater. Interfaces* **2022**, *14* (17), 19505–19514. https://doi.org/10.1021/acsami.2c02228.
(21) Bilardo, R.; Traldi, F.; Vdovchenko, A.; Resmini, M. Influence of Surface Chemistry and Morphology of Nanoparticles on Protein Corona Formation. *Wiley Interdiscip. Rev. Nanomed. Nanobiotechnol.* **2022**, *14* (4), e1788. https://doi.org/10.1002/wnan.1788.
(22) Heinz, H.; Pramanik, C.; Heinz, O.; Ding, Y.; Mishra, R. K.; Marchon, D.; Flatt, R. J.; Estrela-Lopis, I.; Llop, J.; Moya, S.; Ziolo, R. F. Nanoparticle Decoration with Surfactants: Molecular Interactions, Assembly, and Applications. *Surf. Sci. Rep.* **2017**, *72* (1), 1–58. https://doi.org/10.1016/j.surfrep.2017.02.001.
(23) Bragg, W. H. The Structure of Magnetite and the Spinels. *Nature* **1915**, *95* (2386), 561–561. https://doi.org/10.1038/095561a0.
(24) Chatzigoulas, A.; Karathanou, K.; Dellis, D.; Cournia, Z. NanoCrystal: A Web-Based Crystallographic Tool for the Construction of Nanoparticles Based on Their Crystal Habit. *J. Chem. Inf. Model.* **2018**, *58* (12), 2380–2386. https://doi.org/10.1021/acs.jcim.8b00269.

(25) Huan, T. D.; Ramprasad, R. Polymer Structure Prediction from First Principles. *J. Phys. Chem. Lett.* **2020**, *11* (15), 5823–5829. https://doi.org/10.1021/acs.jpclett.0c01553.
(26) Hanwell, M. D.; Curtis, D. E.; Lonie, D. C.; Vandermeersch, T.; Zurek, E.; Hutchison, G. R. Avogadro: An Advanced Semantic Chemical Editor, Visualization, and Analysis Platform. *J. Cheminformatics* **2012**, *4* (1), 17. https://doi.org/10.1186/1758-2946-4-17.
(27) Van Der Spoel, D.; Lindahl, E.; Hess, B.; Groenhof, G.; Mark, A. E.; Berendsen, H. J. C. GROMACS: Fast, Flexible, and Free. *J. Comput. Chem.* **2005**, *26* (16), 1701–1718. https://doi.org/10.1002/jcc.20291.
(28) Hess, B.; Kutzner, C.; van der Spoel, D.; Lindahl, E. GROMACS 4: Algorithms for Highly Efficient, Load-Balanced, and Scalable Molecular Simulation. *J. Chem. Theory Comput.* **2008**, *4* (3), 435–447. https://doi.org/10.1021/ct700301q.
(29) Berendsen, H. J. C.; Postma, J. P. M.; van Gunsteren, W. F.; DiNola, A.; Haak, J. R. Molecular Dynamics with Coupling to an External Bath. *J. Chem. Phys.* **1984**, *81* (8), 3684–3690. https://doi.org/10.1063/1.448118.
(30) Essmann, U.; Perera, L.; Berkowitz, M. L.; Darden, T.; Lee, H.; Pedersen, L. G. A Smooth Particle Mesh Ewald Method. *J. Chem. Phys.* **1995**, *103* (19), 8577–8593. https://doi.org/10.1063/1.470117.
(31) Darden, T.; York, D.; Pedersen, L. Particle Mesh Ewald: An N·log(N) Method for Ewald Sums in Large Systems. *J. Chem. Phys.* **1993**, *98* (12), 10089–10092. https://doi.org/10.1063/1.464397.
(32) Hess, B.; Bekker, H.; Berendsen, H. J. C.; Fraaije, J. G. E. M. LINCS: A Linear Constraint Solver for Molecular Simulations. *J. Comput. Chem.* **1997**, *18* (12), 1463–1472. https://doi.org/10.1002/(SICI)1096-987X(199709)18:12<1463::AID-JCC4>3.0.CO;2-H.
(33) Pascal, T. A.; Goddard, W. A.; Jung, Y. Entropy and the Driving Force for the Filling of Carbon Nanotubes with Water. *Proc. Natl. Acad. Sci.* **2011**, *108* (29), 11794–11798. https://doi.org/10.1073/pnas.1108073108.
(34) Pascal, T. A.; Lin, S.-T.; Goddard Iii, W. A. Thermodynamics of Liquids: Standard Molar Entropies and Heat Capacities of Common Solvents from 2PT Molecular Dynamics. *Phys. Chem. Chem. Phys.* **2011**, *13* (1), 169–181. https://doi.org/10.1039/c0cp01549k.
(35) Lin, S.-T.; Maiti, P. K.; Goddard, W. A. Two-Phase Thermodynamic Model for Efficient and Accurate Absolute Entropy of Water from Molecular Dynamics Simulations. *J. Phys. Chem. B* **2010**, *114* (24), 8191–8198. https://doi.org/10.1021/jp103120q.
(36) Lin, S.-T.; Blanco, M.; Goddard, W. A. The Two-Phase Model for Calculating Thermodynamic Properties of Liquids from Molecular Dynamics: Validation for the Phase Diagram of Lennard-Jones Fluids. *J. Chem. Phys.* **2003**, *119* (22), 11792–11805. https://doi.org/10.1063/1.1624057.
(37) Yury Golitsyn; Gerald J. Schneider; Kay Saalwächter. Reduced-Mobility Layers with High Internal Mobility in Poly(Ethylene Oxide)–Silica Nanocomposites. *J. Chem. Phys.* **2017**, *146* (20), 203303. https://doi.org/10.1063/1.4974768.
(38) C. Tang; X. Li; J. Hao. Interfacial Hydrogen Bonds and Their Influence Mechanism on Increasing the Thermal Stability of Nano-SiO2-Modified Meta-Aramid Fibres. *polymers* **2017**, *9* (504), 1–18. https://doi.org/doi:10.3390/polym9100504.